TISSUE ENGINEERING: Part C
Volume 26, Number 2, 2020

DOI: 10.1089/ten.tec.2019.0228

termis
Tissue Engineering
& Regenerative Medicine
International Society

METHODS ARTICLE

Early Vascular Cells Improve Microvascularization Within 3D Cardiac Spheroids

Isaree Pitaktong,[1] Cecillia Lui, MD,[2] Justin Lowenthal, MD,[1] Gunnar Mattson, BS,[1] Wei-Hung Jung, PhD,[3] Yang Bai, MD,[2] Enoch Yeung, BDS, MBBS,[2] Chin Siang Ong, MBBS, PhD,[2] Yun Chen, PhD,[3] Sharon Gerecht, PhD,[4] and Narutoshi Hibino, MD, PhD[2]

Introduction: A key obstacle in the creation of engineered cardiac tissues of clinically relevant sizes is limited diffusion of oxygen and nutrients. Thus, there is a need for organized vascularization within a three-dimensional (3D) tissue environment. Human induced pluripotent stem cell (hiPSC)-derived early vascular cells (EVCs) have shown to improve organization of vascular networks within hydrogels. We hypothesize that introduction of EVCs into 3D microtissue spheroids will lead to increased microvascular formation and improve spheroid formation.
Methods: HiPSC-derived cardiomyocytes (CMs) were cocultured with human adult ventricular cardiac fibroblasts (FB) and either human umbilical vein endothelial cells (HUVECs) or hiPSC-derived EVCs for 72 h to form mixed cell spheroids. Three different groups of cell ratios were tested: Group 1 (control) consisted of CM:FB:HUVEC 70:15:15, Group 2 consisted of CM:FB:EVC 70:15:15, and Group 3 consisted of CM:FB:EVC 40:15:45. Vascularization, cell distribution, and cardiac function were investigated.
Results: Improved microvasculature was found in EVC spheroids with new morphologies of endothelial organization not found in Group 1 spheroids. CMs were found in a core-shell type distribution in Group 1 spheroids, but more uniformly distributed in EVC spheroids. Contraction rate increased into Group 2 spheroids compared to Group 1 spheroids.
Conclusion: The triculture of CM, FB, and EVC within a multicellular cardiac spheroid promotes microvascular formation and cardiac spheroid contraction.

Keywords: iPS cells, cardiac tissue, 3D cell culture, angiogenesis, and vasculogenesis

Impact Statement

A key obstacle in the creation of cardiac tissues of clinically relevant sizes is the establishment of microvascular networks to support tissue survival and growth. Thus, there is a need for organized vascularization within a three-dimensional (3D) tissue environment. This study demonstrates a method of using early vascular cells (EVCs) to create 3D cardiac spheroids with increased microvascular formation. These vascularized spheroids can then be used as building blocks to create larger vascularized cardiac constructs. This study also serves to demonstrate the ability of EVCs to balance increased vascularization with maintained cardiac function at specific cell ratios within cardiac spheroids.

Introduction

Heart disease is the single largest cause of death worldwide and causes hundreds of thousands of deaths each year. It is a major health issue with poor prognosis and limited quality of life, leading to acute myocardial infarction and chronic heart failure.[1] There is no treatment that can prevent heart failure postmyocardial infarction, and interventions are mostly to alleviate symptoms and have yet to yield positive outcomes leading to increased survival of heart failure patients.[2] Current medical therapies are unable to regenerate cardiac cells to replace dead tissue in a damaged

[1]Department of Biomedical Engineering, Johns Hopkins University, Baltimore, Maryland.
[2]Department of Cardiac Surgery, Division of Cardiac Surgery, Johns Hopkins Hospital, Baltimore, Maryland.
Departments of [3]Mechanical Engineering, and [4]Chemical and Biomolecular Engineering, Johns Hopkins University, Baltimore, Maryland.

heart.[3] In addition, there are a limited number of donors for patients with severe heart failure in need of transplantation. The goal of cardiac tissue engineering is thus the creation of tissue constructs that can aid in regeneration of damaged heart tissue.

However, with some exceptions, most previous studies in cardiac tissue engineering are of limited size.[4,5] A key obstacle in the creation of cardiac tissues of clinically relevant sizes establishment of functional microvascular networks to support tissue survival and growth.[6] Thus, there is a need for organized vascularization within a three-dimensional (3D) tissue environment. Most studies introduce a 3D endothelial tubular network followed by the addition of pericytes.[7] That is, while endothelial cells have the intrinsic ability to self-assemble into network structures, these structures regress without the recruitment of pericytes which surround and stabilize the microvessels.[7] A study by Richards *et al.* introduced adipose-derived stem cells (ADSCs) in scaffold-free cardiac constructs using a self-assembly strategy, with decent vascular results.[8]

While the standard method is to incorporate separate sources of endothelial cells and pericytes, it is now possible, however, to deliver both cell types early on in one sitting. Our laboratory has developed a bipotent differentiation protocol leading to early vascular cells (EVCs) that consist of platelet-derived growth factor receptor-beta positive/smooth muscle protein 22-alpha positive (PDGFRβ+/SM22α+) pericytes and vascular endothelial cadherin/CD31+ expressing (VECad+/CD31+) endothelial cells.[7,9,10] EVCs can be further differentiated to mature endothelial cells (ECs) or pericytes.[7] When encapsulated in a synthetic hyaluronic acid (HA) hydrogel, EVCs self-assemble to functional 3D vascular networks. These engineered human vascular networks survive implantation, integrate with the host vasculature, and establish blood flow.[7,11]

We hypothesized that culturing EVCs along cardiomyocytes (CMs) and fibroblast (FB) within a multicellular spheroid would similarly promote organization of microvascular networks within cardiac spheroids. CMs are the main cells of the heart, allowing for contraction. Endothelial cells form the interior surfaces of blood vessels and regulate angiogenesis.[12–14] FBs are connective tissue cells that produce constituents of the extracellular matrix[14] and help the cells aggregate into a spheroid.[15] Pericytes, derived from the EVCs, usually regulate blood flow[14] and support blood vessel formation.[16] Each of these cell types communicate with each other, both through direct physical contacts, for example, gap junctions, adherens junctions, and desmosomes,[17] as well as through paracrine signaling.[14] While Richards *et al.* have previously explored these cell types in conjunction with ADSCs in the context of a cardiac spheroid microtissue, additionally demonstrating a ''macrotissue'' assembly, our work with EVCs could replace the human umbilical vein endothelial cell (HUVEC)+ADSC component to allow for a more patient-specific, translatable, implantable endothelial cell source.[8]

The great advantage of using a 3D microtissue model, which maximizes cell-to-cell contact by avoiding the use of biomaterials, is to allow cell aggregation and tissue formation that would mimic the native physiological state.[18] The generation of self-assembled micro-vasculature in a biomaterial-free 3D cardiac environment could prove useful for the creation of larger patient-specific cardiac tissues for regeneration after mass CM loss, such as in the case of myocardial ischemia.

Materials and Methods

Generation of human induced pluripotent stem cell-CMs

The following protocol is one we have previously published, in Ong *et al.*[19] Human induced pluripotent stem cells (hiPSCs) (reprogrammed from the peripheral blood mononuclear cells of a healthy donor) were differentiated into CMs in a basal medium of RPMI/B27-insulin, by temporal modulation of Wnt signaling[20] using small molecules (CHIR99021, Tocris, R&D Systems, Cat. No. 4423, and IWR-1, Sigma-Aldrich, Cat. No. I0161).

While we did not measure the CM differentiation efficiency in this study, we have previously investigated the differentiation efficiency of CMs.[21] In that study, flow cytometry was performed on hiPSC-CMs 14 days post-differentiation using VCAM1, a CM marker. VCAM1, a CM marker, was predominantly expressed (93.2%). Of the 6.7% remaining cells, 1.8% and 1.4% were positive for the vascular and FB markers vascular endothelial growth factor receptor 2 (VEGFR-2) and PDGFRβ. More hiPSC-CM quality control measures (spontaneous beating phenotype, electrical connections by voltage optical mapping), are described in that article.

HiPSC-derived CMs were used 21–30 days after differentiation. Before use, each plate of CMs was graded on a scale of A–C, in which A indicated the entire well beat (not necessarily in synchrony), B indicated that some patches of CMs were beating and other patches were not, and C indicated nonbeating wells. The CMs used in this study were all in the A/B range. This grading scale was also used in one of our previous studies.[21]

Generation of EVCs

The following protocol is a slight modification of one we have previously published, in Smith *et al.*2310). Induced pluripotent stem cell (iPSC) lines were passaged every 4 days using Accutase (Sigma-Aldrich) onto six-well plates coated with Geltrex (Life Technologies), passaged into Essential 8 (E8) media (E8; Gibco) with 10 μM ROCK inhibitor Y-27632 (Tocris) at a range of densities aiming for 70–90% confluence in each well after 4 days of culture. E8 media was changed daily, with 2 mL/well at 24 and 48 h postpassage, and 3 mL/well at 72 h postpassage. Differentiation day 0: On day 4 postpassage, with iPSCs at 70–90% confluent, cultures were washed with RPMI 1640 medium with L-glutamine (RPMI; Gibco) and then 3 mL/well differentiation media (RPMI with 2% B-27 minus insulin supplement added +6 μM CHIR-99021 (Selleck). DD2: 48 h after initiation of differentiation, cells were washed with 0.5 mM ethylenediaminetetraacetic acid and then passaged using TrypLE Select (Invitrogen). Cells were passaged onto six-well plates coated with Collagen IV (Corning) at a range of densities ~200 K/well (optimized for each iPSC line). Cells were passaged into Endothelial Cell Differentiation media, composed of Endothelial Cell Growth Medium (PromoCell) supplemented with 10 μM Transforming Growth Factor-β inhibitor SB-431542 (Tocris), 50 ng/mL VEGF (R&D Systems), 2% Fetal

Bovine Serum (PromoCell), and 0.1% Penicillin-Streptomycin (Gibco). When passaging, media was supplemented with 10 μM Y-27632 for plating. DD3 and every 2 days thereafter, media was aspirated and replaced with fresh EC differentiation media (2 mL/well). Cells are ready for harvest via TrypLE and use, analysis, or cryopreservation on DD8. Circular ''clearings'' of endothelial cell colonies will be observed from approximately DD5.

While we did not measure the EVC differentiation efficiency in this study, we have previously investigated the differentiation efficiency of EVCs.[9] In that study, the total yield of VECad+ cells for ROCK inhibitor supplemented differentiation (the same protocol as was used in this study) was 41.76 ± 17.05%. We did not sort or isolate CD31+ or VECad+ expressing cells in this study; rather, we used the EVCs at the differentiation efficiency listed above. This is since it is the combination of cell types, including both endothelial cells and pericytes, which we are investigating.

Other cell types

Human adult ventricular cardiac FBs were obtained from ScienCell (Cat. No. 6310) and maintained with FM-2 medium (ScienCell, Cat. No. 2331) changed every 2 to 3 days. HUVECs were obtained from Lonza (Cat. No. CC-2935).

Spheroid creation

The following protocol is one we have previously published, in Ong *et al.*[19,21] hiPSC-CMs were cocultured with human adult ventricular cardiac FBs and either HUVECs or EVCs in RPMI supplemented with B27 (RPMI 1640 Medium, Invitrogen, Cat. No. 11875-093, and B27 supplement, Thermo Fisher, Cat. No. 17504044) in ultralow adhesion U-bottom 96-well plates (PrimeSurface ultra-low attachment 96-well U-bottom plates, Akita Sumitomo Bakelite Co., Cat. No. MS-9096UZ) at 33,000 cells per well for 72 h to form mixed cell spheroids. This number was chosen based on prior experiments to optimize spheroids for 3D printing.[21] Specifically, combining information about the amount of cardiosphere overlap needed with data about cardiosphere dimensions, we chose to use 33,000 cells per cardiosphere for all subsequent 3D bioprinting experiments, to create cardiospheres that had sufficient overlap for mechanical integrity of the 3D bioprinted cardiac patches.

Group 1 (control) spheroids were created from a CM:FB:HUVEC 70:15:15 ratio, Group 2 spheroids were created from a CM:FB:EVC 70:15:15 ratio, and Group 3 spheroids were created from a CM:FB:EVC 40:15:45 ratio. For a more in-depth explanation for spheroid creation, please see our previously published protocol ''Creation of Cardiac Tissue Exhibiting Mechanical Integration of Spheroids Using 3D Bioprinting.''

Immunofluorescence

Sectioning. Spheroids were fixed in 4% paraformaldehyde and embedded in paraffin before sectioning. Sections are taken at a variety of depths within the spheroid. This arises from the process of spheroid embedding and sectioning. Spheroids are first collected in an empty teabag and then placed in a cassette, which is embedded in wax. However, since the spheroids are free to move around and are not connected to one another, they end up in various vertical positions within the wax. Thus, when the microtome is used to cut a 5 μm section, a single section will contain spheroids at a range of different depths.

The depth of cross sections of individual spheroids can be found given the radius, r, of the cross section, and the radius of the spheroid, R, by using the following equation. For a more in-depth explanation, see Supplementary Figure S1.

$$Depth(\%) = \left(\frac{R - \sqrt{R^2 - r^2}}{2R}\right) \cdot 100\ \%$$

Staining. High-temperature antigen retrieval and paraffin removal were performed by immersing slides in 90% citrate buffer in a pressure cooker for 20 min. A 5% goat serum blocking solution was applied for 30 min. Sections were incubated with primary antibodies to CD31 at 1:50 (Abcam), NG2 at 1:100 (Millipore), Troponin T at 1:100 (Abcam), or Vimentin at 1:100 (Abcam) overnight. Removal of unbound primary antibodies was accomplished by washing using phosphate-buffered saline (PBS). Secondary antibodies (Alexa fluor 488 and 647 anti-rabbit or anti-mouse immunoglobulin G, 1:300; Invitrogen) were incubated with the sections for 1 h before washing using PBS and mounting using VECTASHIELD Antifade Mounting Medium with 4′,6-diamidino-2-phenylindole (Vector Laboratories).

Imaging. Stained sections of 3D cardiac spheroids were imaged using inverted microscopes (EVOS Cell Imaging System). ImageJ software was used to generate composite microscopy images by combining fluorescent channels.

Spheroid size

Spheroid diameters were assessed with the Regenova 3D printer for Group 1 ($n = 80$), Group 2 ($n = 80$), and Group 3 ($n = 78$) spheroids.

Cell viability assay

Viability of FBs, HUVECs, and EVCs was measured before aggregation into spheroids using the Countess automated cell counter. CMs were manually counted (due to the presence of Geltrex fragments in media which would cause an overestimation using the automated cell counter), thus viability was not measured for this population of cells before spheroid formation.

A TUNEL assay (DeadEnd™ Fluorometric TUNEL System; Promega) was used on 3D cardiac spheroids that had been embedded in paraffin and sectioned to determine cell viability. The kit marks apoptotic cells with green fluorescence (fluorescein-12-dUTP is incorporated at 3′-OH DNA ends allowing detection of fragmented DNA of apoptotic cells), and DAPI was used to mark all cells present live and dead. Percent viability calculated as percent of all DAPI-stained cells with green fluorescence from TUNEL stain. Viability was calculated for Group 1 ($n = 7$), Group 2 ($n = 4$), and Group 3 ($n = 3$) spheroids.

Microvascularization assessment

Vascularization in 3D cardiac spheroids was assessed via CD31 IF staining for endothelial cells in two trials in Group 1 ($n=32, 55$), Group 2 ($n=33, 52$), and Group 3 ($n=24, 45$) spheroids. Spheroid images were classified into three distinct morphologies: ''Dispersed'' spheroids, which have no or sparse and scattered CD31-positive cells, ''Clumped'' spheroids, which have scattered clumps of CD31-positive cells and include CD31-positive lumina with thin walls, and ''Clustered'' spheroids, which have organized ''lines'' and/or clusters of CD31-positive cells (Supplementary Table S1). The average counts of each morphology over the trials were compared between spheroid groups. An NG2 stain was also performed in Groups 1, 2, and 3 to detect for pericyte presence.

Cell distribution

CM distribution was assessed from Troponin T stains of Group 1 ($n=7$), Group 2 ($n=5$), and Group 3 ($n=5$) spheroids. FB distribution was assessed from vimentin stains of Group 1 ($n=9$), Group 2 ($n=7$), and Group 3 ($n=6$) spheroids.

Normalized integrated intensities. Images of immunofluorescent-stained sections of cardiac spheroids were analyzed using the ImageJ Radial Profile plugin, which produces a radial plot of normalized integrated intensities around concentric circles as a function of distance from the center of a circular region of interest. Each image of a fluorescently stained spheroid (to Troponin T or vimentin) was first made binary, outliers were removed, then the spheroid of interest was approximated as a circle, and the radial profile plot of integrated fluorescence intensities was obtained (Fig. 3M, N).

Percent composition in spheroid. Average percent composition of cells within spheroid groups was derived from the total normalized integrated fluorescence intensity, using the equation below.

$$Percent\ composition\ in\ spheroid = \left(\frac{1}{255}\frac{1}{N}\sum_{i=1}^{N} x_i\right)\cdot 100\%$$

Normalized integrated fluorescence intensity values, denoted by ''x'' above, are a measure of the ''density'' of cells at a specific radial location. For each spheroid, these values were summed over the entire radius of the spheroid to give the total normalized integrated intensity $\sum_{i=1}^{N} x_i$, a measure of the ''density'' of cells in the entire spheroid. This summed value was then normalized by dividing by the number of samples, or intensity values taken for that spheroid image, N. The value was also divided by the maximum fluorescence intensity value of 255 to obtain the actual percentage of the spheroid occupied by the cell.

Inner/outer ratio. Normalized integrated intensity data were divided into an inner core (spheroid center to half-radius) and outer shell (half-radius to outer edge), then summed for ''inner'' and ''outer.'' Dividing the summed ''inner'' integrated intensity by the summed ''outer'' integrated intensity gave the calculated inner:outer ratio for each spheroid image analyzed.

Functional testing

Particle preparation. Protein G-coated fluorescent particles (38–44 μm in diameter, polystyrene, Spherotech, Inc., Cat. No. PGFP-40052-5) were washed and resuspended in PBS to reach particle density of 0.01% (w/v). Anti-CD106 (VCAM-1) Antibody (BioLegend, Cat. No. 919801) was added to the particle solution to achieve 5 μg/mL for final concentration. After 1 h shaking at room temperature, particles were washed twice and then resuspended in PBS to remove unbound antibodies. The particles were separated from the unbound antibodies by centrifuging at 10,000 g for 1 min and then resuspended in PBS. Antibody-conjugated particles were stored at 4°C for later use.

Labeling cardiac spheroids with fluorescent particles. HiPSCs-derived engineered cardiac spheroids from Group 1 ($n=7$), Group 2 ($n=5$), and Group 3 ($n=3$) were labeled with the antibody-conjugated 40 μm particles at the density of 0.001% (w/v). The mixture of the particles and the spheroids were first gently shaken for 3 min to evenly distribute the particles over the spheroids and incubated at 37°C for 12 h before imaging.

Imaging. The particle-decorated engineered cardiac spheroids were imaged using a fluorescence microscope (Leica TCS SP8) with a 10× objective at 18.5 frames per second. The image acquisition was performed with the pixel density of 1392 × 1040 pixels per frame.

Particle tracking. Particles were tracked by the Fiji[22] plugin TrackMate.[23] Particles were detected by applying Laplacian of Gaussian filter with 40-μm as the estimated blob diameter. The detected particles were linked by using the nearest neighbor search tracker. The particle velocity profile was then extracted for analyzing the beats per minute and maximum velocity of cardiac tissue.

Statistical analysis

For all experiments, data were represented graphically as bar charts with error bars, representing the mean with standard deviation. Statistical analysis was performed with unpaired two-tailed t tests. A p-value <0.05 was considered statistically significant. On bar charts, * indicates $p<0.05$, ** indicates $p<0.01$, and *** indicates $p<0.001$.

Results

Spheroid groups

We created three groups of multicellular spheroids composed of CMs for the primary function of the heart, a stromal cell component to secrete ECM for spheroid adhesion (FBs), and an endothelial component for microvessel formation (either HUVECs or EVC).[24] Group 1 spheroids had a cell composition of CM:FB:HUVEC 70:15:15, Group 2 spheroids had a cell composition of CM:FB:EVC 70:15:15, and Group 3 spheroids had a cell composition of CM:FB:EVC 40:15:45.

Group 1 control spheroids were chosen to be the current standard spheroid used in our laboratory for 3D printing, with a cell ratio of CM:FB:HUVEC 70:15:15. We have previously optimized the cell types, cell ratios, and total cell numbers for this spheroid for 3D printing.[21] Specifically, a fixed endothelial cell component of 15% was chosen based on a previous report demonstrating prevascularization of cardiac patches using endothelial cells.[25] Cardiospheres did not form when only hiPSCs or hiPSC-CMs were used. In the presence of FBs and ECs, hiPSC-CMs formed cardiospheres in 24 h and these cardiospheres started beating spontaneously by 48 h. Tiburcy *et al.* have also previously investigated a CM/non-CM ratio of 70%/30% in the creation of large cardiac constructs and found this ratio to be optimal for contractile force per CM.[5]

Group 2 spheroids consisted of CM:FB:EVC at a 70:15:15 ratio. This was to keep the same cell ratios as the control, only replacing the endothelial component with EVCs to directly compare this spheroid to our current standard and see the effects of EVC compared to HUVEC.

Group 3 spheroids consisted of CM:FB:EVC at a 40:15:45 ratio. This was to see the effect of increasing the ratio of EVC. However, to do this, the percentage of the remaining cellular components had to be decreased. We decided to keep 15% FBs, as we have previously shown in Ong *et al.* that cardiac spheroids are not well formed without FB presence.[21] Thus, the percentage of CMs was decreased instead to maintain the cell ratio.

HUVECs were used as a control in this study, as we were investigating the effects of EVCs, which are a mixed population containing iPSC-ECs with iPSC-pericyte-like cells and other nonendothelial stromal-like cells. This mixed population of cells has been shown to form robust vasculature, partially due to the population of iPSC-ECs and partially due to the supportive effects (both mechanical and paracrine) of the nonendothelial vascular cells.[7] Because our goal was to form robust and functional vasculature in our spheroids, we did not find it necessary to sort to form a pure population of iPSC-ECs. Future work is planned, which will utilize sorted iPSC-ECs and endothelial subtypes; however, we feel that it is beyond the scope of this study.

Spheroid size

Spheroid diameter was on average 608 ± 30 μm for Group 1 ($n = 80$), 596 ± 29 μm for Group 2 ($n = 80$), and 533 ± 92 μm for Group 3 ($n = 78$) spheroids. The average Group 2 spheroid diameter was less than that of Group 1 ($p < 0.01$), and average Group 3 spheroid diameter was both less than that of Group 1 ($p < 0.001$) and less than that of Group 3 ($p < 0.001$) (Fig. 1).

Cell viability

Cell viabilities were found to be 91%, 93%, and 88% for FBs, HUVEC, and EVC, respectively, before spheroid formation.

Spheroid viability was on average $95 \pm 3\%$ for Group 1 ($n = 7$), $97 \pm 0.5\%$ for Group 2 ($n = 4$), and $94 \pm 1\%$ for Group 3 ($n = 5$). Group 3 spheroid viability was found to be less than that for Group 2 ($p < 0.001$), but not significantly different from Group 1 (Fig. 1). Furthermore, dead cells were not localized to the center of the spheroid, but rather scattered throughout.

Cross section diameter of imaged TUNEL-stained spheroids varied from 200 to 500 μm. However, average spheroid diameters in this study (measured by the Regenova 3D printer scanning function) were around 500 μm, thus

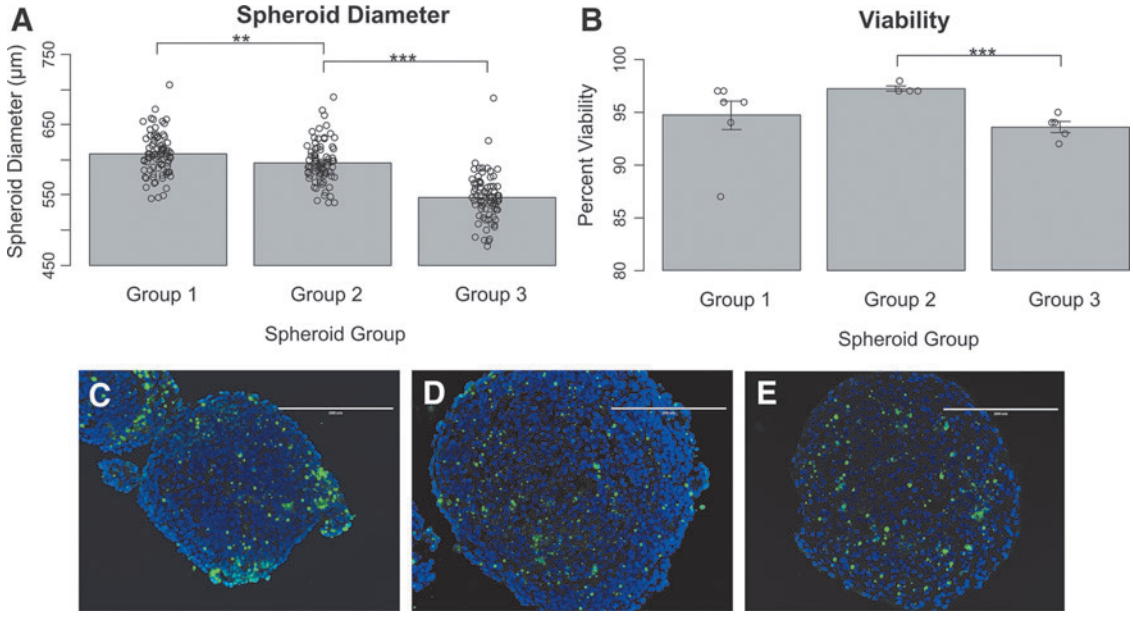

FIG. 1. Spheroid size and viability for Group 1 (CM:FB:HUVEC 70:15:15), Group 2 (CM:FB:EVC 70:15:15), and Group 3 (CM:FB:EVC 40:15:45) spheroids. **(A)** Average spheroid diameter. **(B)** Average spheroid viability. **(C–E)** TUNEL stains for **(C)** Group 1, **(D)** Group 2, and **(E)** Group 3 spheroids. *Blue* DAPI stain indicates all cells present live and dead. *Green* TUNEL stain for fluorescein-12-dUTP at 3′-OH DNA ends indicates apoptotic cells. On bar charts, $^{**}p < 0.01$, and $^{***}p < 0.001$. CM, cardiomyocyte; DAPI, 4′,6-diamidino-2-phenylindole; EVC, early vascular cell; FB, fibroblast; HUVEC, human umbilical vein endothelial cell.

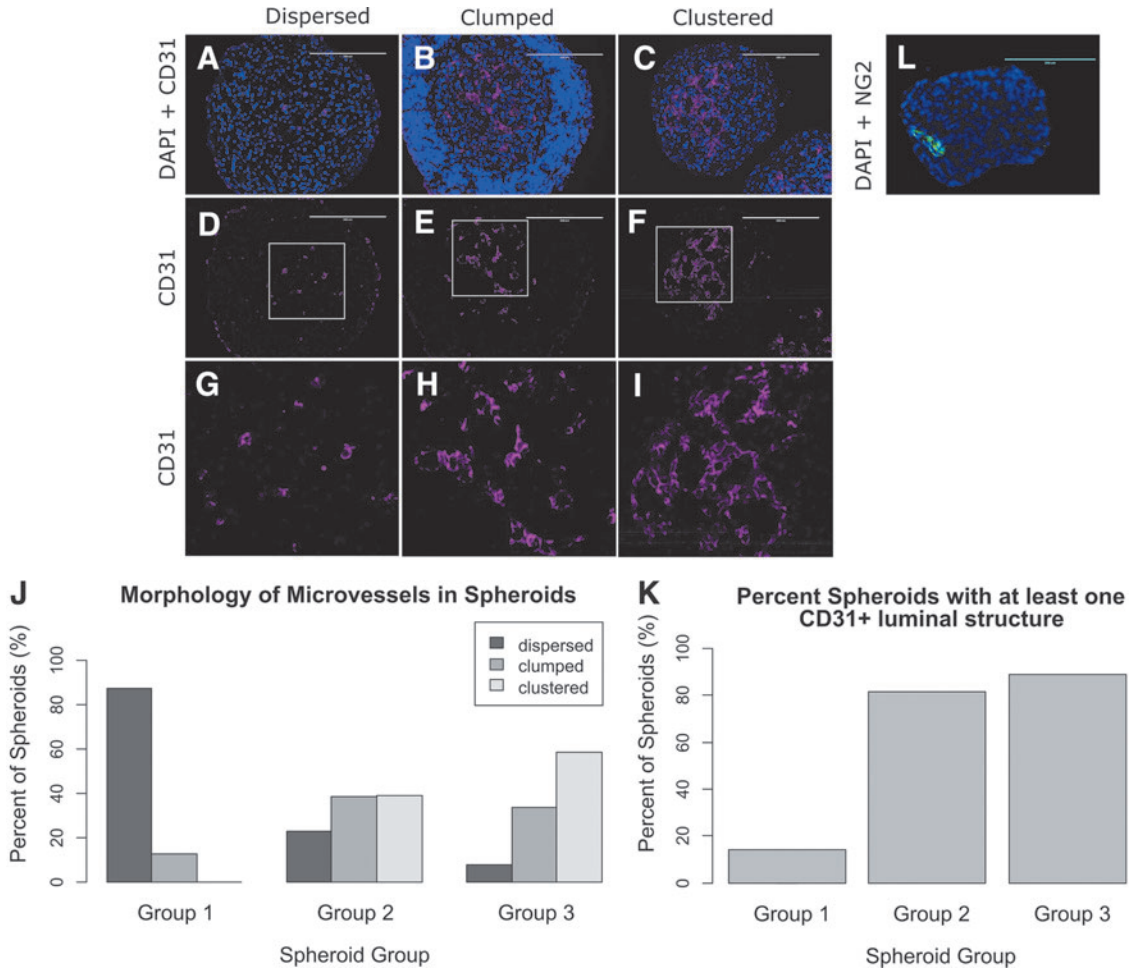

FIG. 2. **(A–I)** Spheroids were categorized by morphology into three groups. *Purple* = CD31, *blue* = DAPI. Scale bar in **(A–F)**: 200 μm. Image size for **(G–I)**: 200 × 200 μm. **(A, D, G)** ''Dispersed'' spheroids have no or sparse and scattered CD31-positive cells. **(B, E, H)** ''Clumped'' spheroids have scattered clumps of CD31-positive cells and include CD31-positive lumina with thin walls. **(C, F, I)** ''Clustered'' spheroids have organized ''lines'' and/or clusters of CD31-positive cells. **(J)** Comparison of microvessel morphology between spheroids groups. **(K)** Quantification of spheroid groups with at least one CD31 positive luminal structure per group. **(L)** NG2 stain for pericytes in a Group 2 EVC spheroid. *Green* = NG2, *blue* = DAPI. Scale bar: 200 μm.

these cross sections were from spheroids at depths ranging from ~5% to 50% of the spheroid, where 50% would be a cross section through the center of the spheroid. Given this fact, the average spheroid viability taken represents an average of viability at varying depths throughout the spheroid. In addition, the low standard deviation found associated with the mean indicates that viability was not drastically different at these different depths, suggesting that cell viability does not change greatly with depth.

Microvascularization within spheroids

A CD31 stain for endothelial cells was performed to assess microvascularization within Group 1 ($n = 32$, 55), Group 2 ($n = 33$, 52), and Group 3 ($n = 24$, 45) spheroids.

Spheroids were categorized by morphology into three groups—''dispersed,'' ''clumped,'' and ''clustered'' (Fig. 2). Group 1 included spheroids with only ''dispersed'' (88%) and ''clumped'' (13%) morphologies. EVC spheroids included two additional morphologies not seen in Group 1. That is, 39% of Group 2 spheroids and 59% of Group 3 spheroids were classified as ''clustered,'' morphologies not seen in Group 1. In addition, Groups 2 and 3 included fewer ''dispersed'' spheroids compared to Group 1 (23% and 8%, respectively) (Fig. 2J; Table 1).

Groups 2 and 3 spheroids had more CD31-positive lumina (81 ± 18% and 89 ± 10%, respectively), than Group 1 spheroids (13 ± 19%) (Fig. 2K).

TABLE 1. MORPHOLOGY OF MICROVESSELS IN SPHEROIDS

Morphology	*Group 1*	*Group 2*	*Group 3*
Dispersed	88 ± 13%	23 ± 4%	8 ± 3%
Clumped	13 ± 13%	38 ± 2%	34 ± 13%
Clustered	0 ± 0%	39 ± 6%	59 ± 16%

Values after a ± indicate standard error of the mean. Spheroids Table 1 were categorized by morphology into four groups—''dispersed,'' ''clumped,'' ''clustered,'' and ''lumen thick wall.'' Values in the table indicate the average percentage of spheroids in a group with the indicated morphology.

An NG2 stain was performed to assess for pericyte present within the three groups. Although not found in Group 1, organized NG2-positive cells were found in EVC spheroids (Fig. 2L). This is supported by a study, in which EVCs formed multicellular networks within HA hydrogels, where instances of NG2 pericytes were incorporated in the luminal structures and encircling the forming tubular structures.[11]

Cell distribution

Troponin T stains were performed to assess CM distribution within Groups 1, 2, and 3 spheroids (more information in Materials and Methods section) (Fig. 3A–F). The average inner/outer ratio was 0.27 ± 0.09 for Group 1 spheroids ($n = 7$), 0.4 ± 0.1 for Group 2 spheroids ($n = 5$), and 0.4 ± 0.3 for Group 3 spheroids ($n = 5$). Group 2 had a significantly greater inner/outer ratio than Group 1 ($p = 0.032$), indicating the distribution of CMs was more uniform in Group 2 spheroids, despite both groups containing the same initial ratio of CMs (70%). However, the ratio was still <1, indicating the presence of a greater concentration of CMs toward the outer edge of the spheroid. Group 3 spheroids had a large variation in inner/outer ratios, which may be attributed to the much lower percentage of CMs (40%) in its composition compared to that of Group 1 or Group 2 (Fig. 3O).

Based on total normalized integrated fluorescence intensity values, Group 2 had the highest percentage composition of Troponin T-positive cells ($30 \pm 4\%$), which was significantly greater than both that of Group 1 ($18 \pm 2\%$, $p = 0.026$) and Group 3 ($11 \pm 2\%$, $p = 0.003$) (Fig. 3Q).

Vimentin stains were performed to assess FB distribution within Groups 1, 2, and 3 spheroids (Fig. 3G–L). The average inner/outer ratio was 1.2 ± 0.7 for Group 1 ($n = 9$), 0.8 ± 0.3 for Group 2 ($n = 7$), and 0.7 ± 0.3 for Group 3 ($n = 6$) spheroids. There was no significant difference between the three groups, and all groups contained the same ratio of FBs (15%). The ratios for vimentin stains are also much closer to one, indicating that FBs were more uniformly distributed throughout the spheroid, regardless of the distribution of CMs (Fig. 3P).

Based on total normalized integrated fluorescence intensity values, all three groups had similar percentage compositions of Vimentin-positive cells. The average percentage compositions were $30 \pm 3\%$, $31 \pm 3\%$, and $29 \pm 7\%$ for Groups 1, 2, and 3 spheroids, respectively (Fig. 3R).

Functional testing

Spheroids contraction rate and maximum contraction velocity were determined for Group 1 ($n = 7$), Group 2 ($n = 5$), and Group 3 ($n = 3$) spheroids. Spheroids spontaneously contracted on average 43 ± 6 beats per minute for Group 1 spheroids. Group 2 spheroids contracted more quickly than Group 1 spheroids, at 55 ± 4 beats per minute ($p < 0.01$), despite having the same ratio of CMs (70%). Group 3 spheroids contracted more slowly than both Group 1 spheroids ($p = 0.010$) and Group 2 spheroids ($p < 0.01$), at 23 ± 12 beats per minute (Fig. 4).

Maximum contraction velocity was $164 \pm 43\ \mu m/s$ for Group 1 spheroids, $221 \pm 82\ \mu m/s$ for Group 2 spheroids, and $106 \pm 47\ \mu m/s$ for Group 3 spheroids. No significant difference was found between the three groups for maximum contraction velocity (Fig. 4).

Discussion

Overall, we have found that the presence of EVCs in 3D multicellular spheroids influences spheroid formation and viability, morphology of microvascular structures and distribution of varying cell types within the spheroid, as well as overall cardiac function of the spheroid. Current cardiac tissue engineering efforts strive to establish functional microvascular networks in cardiac constructs through preestablished endothelial networks, or through endothelial self-assembly followed by the addition of pericytes. However, oftentimes the result is structural regress of any microvascular structures. This study uses EVCs, a type of progenitor cells, which can differentiate into both endothelial cells and pericytes, and have the ability to self-assemble into a bicellular functional vascular network in hydrogels.[7] We found that EVCs representing both endothelial and pericyte-like subtypes were similarly distributed through the spheroids in such a way to suggest possible enhancement of microvascular network formation in a 3D microtissue environment, in coculture with FBs and CMs.

The lower percentage viability of EVCs measured before cell aggregation into spheroids should have resulted in a decreased spheroid viability, yet, we found that EVC spheroids had a higher overall percentage of viable cells. However, we understand that cell viabilities will likely have changed over the subsequent 3 days of culture, during which the process of cell aggregation into a spheroid occurs. While we stained for CMs, FBs, and endothelial cells, we only measured overall viability of all cells in the spheroid without discriminating between individual cell populations; thus, we do not know the relative contribution of each cell type to this viability percentage. The results of such an investigation would be very insightful; however, we leave this to future experimentation as we believe it is beyond the scope of this experiment, which aims only to determine whether the presence of EVCs can improve vasculature without negatively affecting other factors, including cell viability.

We found high viability (>90%) in all spheroid groups despite all groups having average spheroid sizes larger than would be accounted for by the standard diffusion limit of $\sim 200\ \mu m$.[26,27] In addition, we note that cell viability was measured at varying spheroid depths and did not change significantly with depth. Our study compared Group 1 spheroids (which lacked EVCs) to Groups 2 and 3 spheroids (which contained EVCs) to see the effect EVCs had on cell viability. We found that cell viability remained high (>90%) in all spheroid groups, thus from this result alone we cannot conclude whether EVCs affect cell viability. However, we found, in addition, that there was a significantly different distribution of CMs within the spheroid. Thus, we hypothesize that EVCs may play a role in maintaining an even CM distribution within the spheroid while keeping viability high.

It has been shown that CMs on preformed endothelial cell networks exhibited significantly less CM apoptosis compared with simultaneous EC-CM seeding, and conditioned medium has also shown to decrease myocyte necrosis.[28] Thus, it is possible that even without the actual delivery of nutrients, the organization of endothelial cells in EVC spheroid groups had a prosurvival effect on CMs due to local interactions and direct signaling between the two cell types. Other factors may also have improved oxygen and

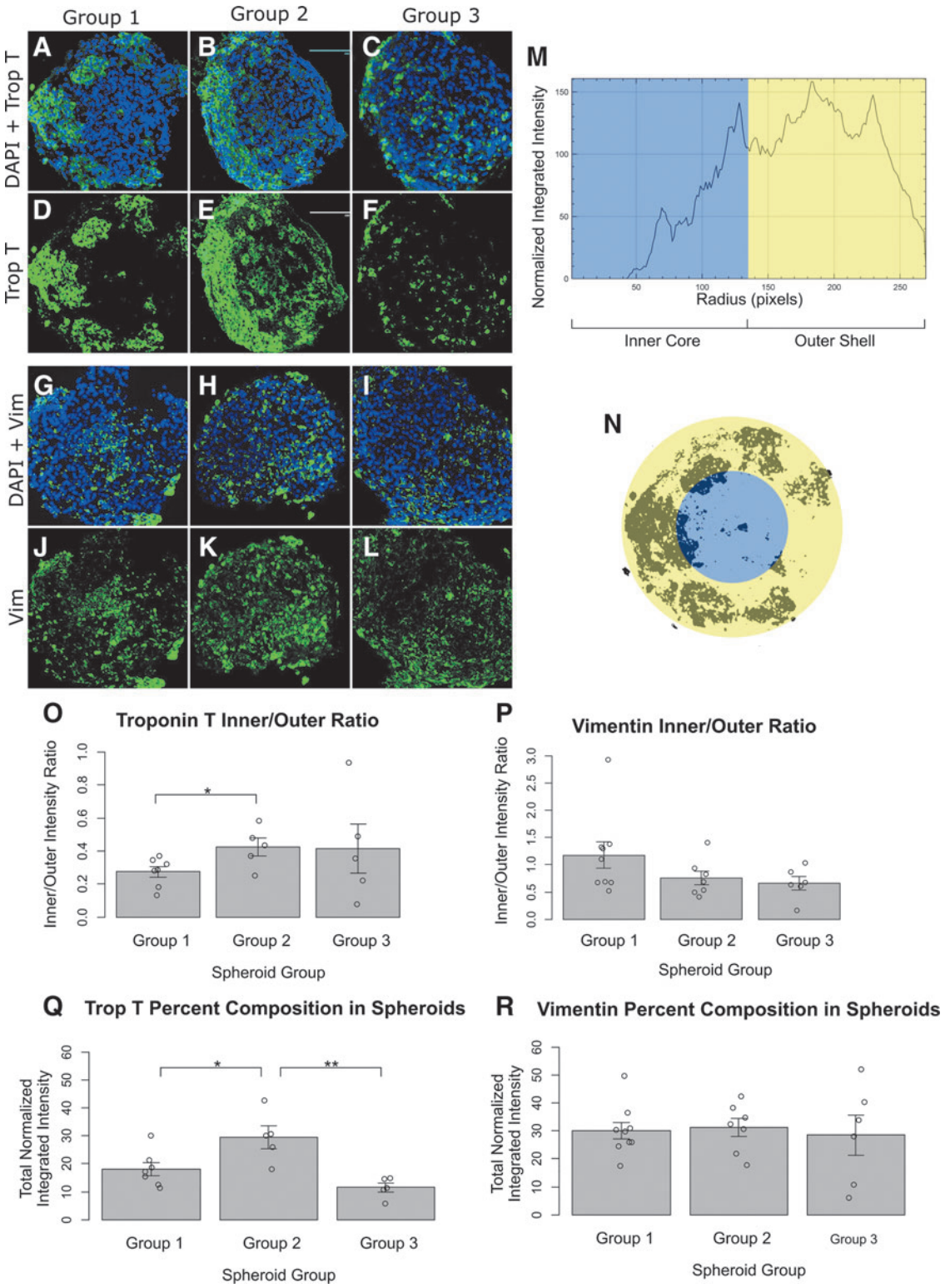

FIG. 3. Distribution of cell types within spheroids. Image size: 400 × 400 μm. **(A–F)** Troponin T stain for cardiomyocytes. *Green* = Troponin T, *blue* = DAPI. **(G–L)** Vimentin stain for fibroblasts. *Green* = Vimentin T, *blue* = DAPI. **(A, D, G, L)** Group 1 spheroid (CM:FB:HUVEC 70:15:15). **(B, E, H, K)** Group 2 spheroid (CM:FB:EVC 70:15:15). **(C, F, I, L)** Group 3 spheroid (CM:FB:EVC 40:15:45). **(M, N)** Illustration depicting method of generating inner/outer ratio using Troponin T and vimentin stains. **(M)** Normalized integrated fluorescence intensity along concentric *circles* was obtained with the ImageJ Radial Profile Plot plugin. **(N)** The plot was divided at half-radius corresponding to an ''inner core'' (*blue*) and ''outer shell'' (*yellow*) for the spheroid. Dividing the resulting sums of integrated intensities gives the ''inner/outer ratio.'' **(O, P)** Inner/outer ratio obtained from **(O)** Troponin T stains for cardiomyocytes, and **(P)**, vimentin stains for fibroblasts. **(Q, R)** Percent composition of **(Q)** Troponin T-positive cells and **(R)** vimentin-positive cells derived from normalized integrated fluorescence intensity data. On bar charts, $*p < 0.05$, $**p < 0.01$.

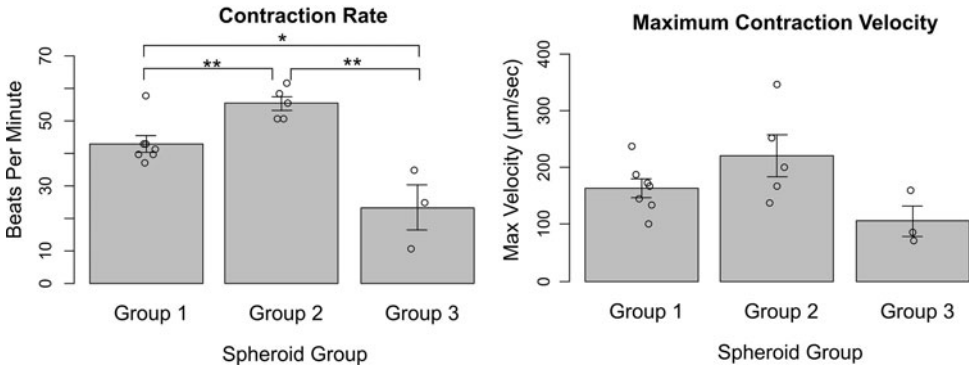

FIG. 4. Contraction rate and maximum velocity for Group 1 (CM:FB:HUVEC 70:15:15), Group 2 (CM:FB:EVC 70:15:15), and Group 3 (CM:FB:EVC 40:15:45) spheroids. On bar charts, $*p<0.05$, $**p<0.01$.

nutrient diffusion, such as the spontaneous contraction of spheroids.[29] The cells in spheroids—hiPSC-derived cells and FBs—may also exhibit a greater tolerance to hypoxia.[30]

Based on the range of spheroid depths, at which we sectioned and found CD31+ luminal structural, we observed CD31 staining patterns throughout the depth of spheroids suggestive of network formation upon replacing the endothelial component of the cardiac spheroids with EVCs. Specifically, a new more organized morphology of endothelial cell structure (''clustered'') was seen in EVC spheroids. This may be due to the presence of pericytes, differentiated from EVCs, supporting vasculature. It is also possible that since CMs already secrete cardiokines promoting angiogenesis such as VEGF, paracrine signaling between the pericytes and other cell types triggered further release of factors promoting angiogenesis. However, the paracrine interactions of pericytes with CMs have not been well documented.[14]

We did not investigate stability of endothelial networks in this study, as the aim of this study was to create vascularized spheroids for use as building blocks within 3D printed cardiac patches. However, this would be an excellent future study upon the creation of the printed cardiac patches to determine stability and function of endothelial networks and integration with host vasculature. We have also previously performed studies on these EVCs in hydrogels, in which we found that these EVCs self-organize to form microvascular networks in an engineered matrix, and that these engineered human vascular networks survive implantation, integrate with the host vasculature, and establish blood flow.[7]

With HUVECs forming the endothelial portion of Group 1 spheroids, CMs were found to aggregate at the outer shell of these spheroids. With the presence of EVCs, however, CMs were much more uniformly distributed throughout the spheroid. A potential cause of this change in cell distribution is that increased vascularization in EVC spheroids enabled delivery of more nutrients to the center of the spheroid creating a more favorable environment for CMs to reside in, and thus CMs in non-EVC groups migrated to the outer shell to avoid the more hypoxic conditions in the spheroid core. However, iPSC-derived CMs are still functionally immature after differentiation,[31] and it has been shown that neonatal CMs are more resistant to hypoxia.[32] Thus, it is possible that new physical contacts or paracrine signaling were introduced with the addition of EVCs that caused the change in CM distribution. For example, another study found that capillary-like networks formed by endothelial cells promoted CM reorganization along the EC structures.[28] Another potential cause of the aggregation of CMs along the outer edge in non-EVC spheroids is hypoxia-induced FB proliferation in the spheroid core, promoting CM distribution on the outer edges.[33]

Given the same input ratio of CMs (70%), we found spheroids with EVCs to have greater contraction rate compared to non-EVC groups. It is important to note that despite starting with the same percent composition of CMs in culture, this percent composition increased in EVC spheroids, compared to non-EVC spheroids. Thus, it could be this greater percent composition of CMs that is resulting in the increase in function. However, the more uniform distribution of CMs in EVC groups may also have contributed to the greater contraction rate in these groups. It is also possible that the increased organization of endothelial structures in EVC groups played a role in promoting contraction. A study by Narmoneva *et al.* found that preformed endothelial cell networks promoted coordinated, spontaneous contraction of CMs in peptide hydrogels as well as increased connexin 43 expression.[28] Furthermore, even the presence of EVCs may aid in contraction via paracrine signaling. Studies have found the addition of FBs and cardiac endothelial cells to CMs within spheroid microtissues to enhance spontaneous contraction rate.[34] Even HUVECs have shown to improve the contractile capacity of murine microtissues.[35] Since endothelial cells secrete cardiac angiocrines, including those that can regulate CM contractility[36] (e.g., nitric oxide,[36] endothelin-1[37]), it is possible that EVCs secrete a greater amount or variety of factors promoting CM contractility than HUVECs.

Group 3 spheroids contracted more slowly than both Group 1 spheroids and Group 2 spheroids. However, this could be attributed to the much smaller ratio of CMs in Group 3 (40% initially) compared to that of Group 1 or Group 2 (70% initially). Our results are consistent with those of Devarasetty *et al.*, which also investigated contraction within cardiac organoids and found a baseline beating rate of 30 beats per minute.[38] This is within the range of contraction rates found in our study.

Few reports have described the physical shortening of scaffold-free 3D cardiac structures. However, Mukae *et al.* investigated multicellular spheroids of CMs and neural progenitor cells.[39] They found a contractile velocity of 110 ± 60 μm/s at a 70:30 ratio of CMs to neural progenitor cells. This is just slightly below the contractile velocity we found in our Groups 1 and 2 spheroids (which similarly contained 70% CMs). Mukae *et al.*[39] also showed that adding hiPSC-neural progenitor cells did not have a negative effect on the contractile function of cardiac cells until the ratio of CM:NP reached 70:30. We found a similar result, where contractile velocity fell for Group 3 spheroids,

when the CM:EVC ratio became 40:45, although this drop was not significant.

A balance is required between the ratio of EVCs and CMs in the spheroid to achieve optimal microvascularization while maintaining cardiac function. That is, Group 3 spheroids (consisting of 45% EVC for the endothelial component) had a significantly greater percentage of spheroids with at least one CD31-positive luminal structure in addition to the presence of a ''clustered'' morphology in comparison to control spheroids (consisting of 15% HUVEC for endothelial component). However, with only 40% CM, Group 3 spheroids also had significantly lower contraction rates than both Groups 1 and 2 spheroids, both of which consisted of 70% CMs. Thus, while increasing the percentage of EVCs may improve microvascularization, any resulting decreases in the percentage of CMs also result in decreased cardiac function of the spheroid. Another factor in the vascular formation and cardiac function derived from EVCs is the difference in mechanical environment. For example, previous hydrogel studies have been performed with controlled stiffness,[40,41] whereas in this scaffold-free study stiffness depends on cell behavior and ECM formation. Vascular network formation has also previously been evaluated in suspension-cultured cardiovascular organoids (although this was later improved with stiffness-controlled hydrogels).[42]

One limitation of the study is the short duration of spheroid culture. Another is that no electrical studies were performed on the spheroid. In addition, only one marker was used to identify pericytes, but multiple markers should be used to identify this cell type. Furthermore, the immaturity of iPSC-derived cells has been established and is an ongoing obstacle in research using iPSCs. Another limitation of using EVCs is less control over the cell source compared to presorted hiPSC-ECs or HUVECs with the addition of iPSC-pericytes, since there is not data on how many endothelial/pericytes are differentiated each time *in situ* and thus batch-to-batch consistency may be an issue.

In conclusion, the presence of EVCs within a multicellular cardiac spheroid promotes microvascular formation and cardiac spheroid contraction. An optimal cell ratio within the spheroid is required to balance increased vascularization with cardiac function, which was best achieved by Group 2 spheroids (CM:FB:EVC 70:15:15) in this study.

Disclosure Statement

No competing financial interests exist.

Funding Information

Funding was provided by the Magic That Matters Fund for Cardiovascular Research at Johns Hopkins Hospital.

Supplementary Material

Supplementary Figure S1
Supplementary Table S1

References

1. Benjamin, E.J., Muntner, P., Alonso, A., *et al.* Heart disease and stroke statistics—2019 update: a report from the American Heart Association. Circulation **139,** e56, 2019.
2. Kitsara, M., Agbulut, O., Kontziampasis, D., Chen, Y., and Menasché, P. Fibers for hearts: a critical review on electrospinning for cardiac tissue engineering. Acta Biomater **48,** 20, 2017.
3. Ji, S.T., Kim, H., Yun, J., Chung, J.S., and Kwon, S.-M. Promising therapeutic strategies for mesenchymal stem cell-based cardiovascular regeneration: From cell priming to tissue engineering. Stem Cells Int **2017,** 1, 2017.
4. Achilli, T., Meyer, J., and Morgan, J.R. Advances in the formation, use and understanding of multi-cellular spheroids. Expert Opin Biol Ther **12,** 1347, 2012.
5. Tiburcy, M., Hudson, J.E., Balfanz, P., *et al.* Defined engineered human myocardium with advanced maturation for applications in heart failure modeling and repair. Circulation **135,** 1832, 2017.
6. Discher, D.E., Mooney, D.J., and Zandstra, P.W. Growth factors, matrices, and forces combine and control stem cells. Science (80-.) **324,** 1673, 2009.
7. Kusuma, S., Shen, Y.-I., Hanjaya-Putra, D., Mali, P., Cheng, L., and Gerecht, S. Self-organized vascular networks from human pluripotent stem cells in a synthetic matrix. Proc Natl Acad Sci U S A **110,** 12601, 2013.
8. Richards, D.J., Coyle, R.C., Tan, Y., *et al.* Inspiration from heart development: biomimetic development of functional human cardiac organoids. Biomaterials **142,** 112, 2017.
9. Chan, X.Y., Black, R., Dickerman, K., *et al.* Three-dimensional vascular network assembly from diabetic patient-derived induced pluripotent stem cells. Arterioscler Thromb Vasc Biol **35,** 2677, 2015.
10. Smith, Q., Macklin, B., Chan, X.Y., *et al.* Differential HDAC6 activity modulates ciliogenesis and subsequent mechanosensing of endothelial cells derived from pluripotent stem cells. Cell Rep **24,** 895, 2018.
11. Hanjaya-Putra, D., Bose, V., Shen, Y.I., *et al.* Controlled activation of morphogenesis to generate a functional human microvasculature in a synthetic matrix. Blood **118,** 804, 2011.
12. Aird, W.C. Phenotypic heterogeneity of the endothelium. Circ Res **100,** 158, 2007.
13. Aird, W.C. Endothelial cell heterogeneity. Cold Spring Harb Perspect Med **2,** 1, 2012.
14. Talman, V., and Kivelä, R. Cardiomyocyte—endothelial cell interactions in cardiac remodeling and regeneration. Front Cardiovasc Med **5,** 1, 2018.
15. Salmenperä, P., Kankuri, E., Bizik, J., *et al.* Formation and activation of fibroblast spheroids depend on fibronectin-integrin interaction. Exp Cell Res **314,** 3444, 2008.
16. Bergers, G., and Song, S. The role of pericytes in blood-vessel formation and maintenance. Neuro Oncol **7,** 452, 2005.
17. Noorman, M., van der Heyden, M.A.G., van Veen, T.A.B., *et al.* Cardiac cell-cell junctions in health and disease: electrical versus mechanical coupling. J Mol Cell Cardiol **47,** 23, 2009.
18. de Boer, J., van Blitterswijk, C., Fennema, E., Rouwkema, J., and Rivron, N. Spheroid culture as a tool for creating 3D complex tissues. Trends Biotechnol **31,** 108, 2013.
19. Ong, C.S., Fukunishi, T., Nashed, A., *et al.* Creation of cardiac tissue exhibiting mechanical integration of spheroids using 3D bioprinting. J Vis Exp **125,** 1, 2017.
20. Lian, X., Hsiao, C., Wilson, G., *et al.* Cozzarelli prize winner: robust cardiomyocyte differentiation from human pluripotent stem cells via temporal modulation of canonical Wnt signaling. Proc Natl Acad Sci U S A **109,** E1848, 2012.

21. Ong, C.S., Fukunishi, T., Zhang, H., *et al.* Biomaterial-free three-dimensional bioprinting of cardiac tissue using human induced pluripotent stem cell derived cardiomyocytes. Sci Rep **7,** 4566, 2017.
22. Schindelin, J., Arganda-Carreras, I., Frise, E., *et al.* Fiji: an open-source platform for biological-image analysis. Nat Methods **9,** 241, 2009.
23. Jaqaman, K., Loerke, D., and Mettlen, M. Robust single particle tracking in live cell time-lapse sequences. Nat Methods **5,** 695, 2008.
24. Polonchuk, L., Chabria, M., Badi, L., *et al.* Cardiac spheroids as promising in vitro models to study the human heart microenvironment. Sci Rep **7,** 7005, 2017.
25. Noguchi, R., Nakayama, K., Itoh, M., *et al.* Development of a three-dimensional pre-vascularized scaffold-free contractile cardiac patch for treating heart disease. J Hear Lung Transplant **35,** 137, 2016.
26. Ruei-Zeng, L., and Hwan-You, C. Recent advances in three-dimensional multicellular spheroid culture for biomedical research. Biotechnol J **3,** 1172, 2008.
27. Cui, X., Hartanto, Y., and Zhang, H. Advances in multicellular spheroids formation. J R Soc Interface **14,** pii: 20160877, 2017.
28. Narmoneva, D.A., Vukmirovic, R., Davis, M.E., Kamm, R.D., and Lee, R.T. Endothelial cells promote cardiac myocyte survival and spatial reorganization. Circulation **110,** 962, 2004.
29. Noguchi, R., Itoh, M., Kamohara, K., *et al.* Development of a three-dimensional pre-vascularized scaffold-free contractile cardiac patch for treating heart disease. J Hear Lung Transplant **35,** 137, 2016.
30. Lee, J.H., Han, Y.S., and Lee, S.H. Long-duration three-dimensional spheroid culture promotes angiogenic activities of adipose-derived mesenchymal stem cells. Biomol Ther **24,** 260, 2016.
31. Koivumäki, J.T., Naumenko, N., Tuomainen, T., *et al.* Structural immaturity of human iPSC-derived cardiomyocytes: in silico investigation of effects on function and disease modeling. Front Physiol **9,** 1, 2018.
32. Pyo, J.O., Nah, J., Kim, H.J., *et al.* Protection of cardiomyocytes from ischemic/hypoxic cell death via Drbp1 and pMe 2 GlyDH in cardio-specific ARC transgenic mice. J Biol Chem **283,** 30707, 2008.
33. Senavirathna, L.K., Huang, C., Yang, X., *et al.* Hypoxia induces pulmonary fibroblast proliferation through NFAT signaling. Sci Rep **8,** 1, 2018.
34. Ravenscroft, S.M., Pointon, A., Williams, A.W., Cross, M.J., and Sidaway, J.E. Cardiac non-myocyte cells show enhanced pharmacological function suggestive of contractile maturity in stem cell derived cardiomyocyte microtissues. Toxicol Sci **152,** 99, 2016.
35. Garzoni, L.R., Rossi, M.I.D., de Barros, A.P.D.N., *et al.* Dissecting coronary angiogenesis: 3D co-culture of cardiomyocytes with endothelial or mesenchymal cells. Exp Cell Res **315,** 3406, 2009.
36. Brutsaert, D.L. Cardiac endothelial-myocardial signaling: its role in cardiac growth, contractile performance, and rhythmicity. Physiol Rev **83,** 59, 2015.
37. Drawnel, F.M., Archer, C.R., and Roderick, H.L. The role of the paracrine/autocrine mediator endothelin-1 in regulation of cardiac contractility and growth. Br J Pharmacol **168,** 296, 2013.
38. Devarasetty, M., Forsythe, S., Shupe, T.D., *et al.* Optical tracking and digital quantification of beating behavior in bioengineered human cardiac organoids. Biosensors **7,** 24, 2017.
39. Mukae, Y., Itoh, M., Noguchi, R., *et al.* The addition of human iPS cell-derived neural progenitors changes the contraction of human iPS cell-derived cardiac spheroids. Tissue Cell **53,** 61, 2018.
40. Smith, Q., Rochman, N., Carmo, A.M., *et al.* Cytoskeletal tension regulates mesodermal spatial organization and subsequent vascular fate. Proc Natl Acad Sci U S A **115,** 8167, 2018.
41. Smith, Q., Chan, X.Y., Carmo, A.M., Trempel, M., Saunders, M., and Gerecht, S. Compliant substratum guides endothelial commitment from human pluripotent stem cells. Sci Adv **3,** e1602883, 2017.
42. Shkumatov, A., Baek, K., and Kong, H. Matrix rigidity-modulated cardiovascular organoid formation from embryoid bodies. PLoS One **9,** 1, 2014.

Address correspondence to:
Narutoshi Hibino, MD, PhD
Department of Surgery
Division of Cardiac Surgery
University of Chicago Medicine
5841 S. Maryland Ave
Room E500B | MC5040
Chicago, IL 60637

E-mail: nhibino@surgery.bsd.uchicago.edu

Received: August 21, 2019
Accepted: December 9, 2019
Online Publication Date: January 31, 2020